Catalysis Today 148 (2009) 109–114

Contents lists available at ScienceDirect

Catalysis Today

journal homepage: www.elsevier.com/locate/cattod

Sol–gel silver hexatitanates as photocatalysts for the 4-chlorophenol decomposition

V. Rodríguez-González [a,*], M.A. Ruiz-Gómez [a], L.M. Torres-Martínez [a], R. Zanella [b], R. Gómez [c]

[a] Universidad Autónoma de Nuevo León, Facultad de Ingeniería Civil, Instituto de Ingeniería Civil, Depto. de Ecomateriales y Energía, Av. Universidad S/N, San Nicolás de los Garza, Nuevo León, C.P. 66451, Mexico
[b] Centro de Ciencias Aplicadas y Desarrollo Tecnológico, Universidad Nacional Autónoma de México, Circuito Exterior S/N, Ciudad Universitaria, A.P. 70-186, C.P. 04510, México D.F., Mexico
[c] Universidad Autónoma Metropolitana-I, Depto. de Química, Av. San Rafael Atlixco No. 186, México D.F., C. P. 09340 Mexico

ARTICLE INFO

Article history:
Available online 3 June 2009

Keywords:
Solid state sodium hexatitanates
Sol–gel microfiber synthesis
$Na_2Ti_6O_{13}$ microfibers
4-CP photodecomposition
Silver surface plasmon resonance

ABSTRACT

Sodium hexatitanate ($Na_2Ti_6O_{13}$) and silver-supported sodium hexatitanates were prepared by the sol–gel and solid state reaction methods. Fibril structures and octagonal microbar hexatitanates were obtained. Silver nanoparticles were incorporated into the sodium hexatitanate supports by the deposition–precipitation technique. HRTEM (high resolution transmission electron microscopy) and high angle annular dark field (HAADF) digital images showed silver particles with nanometric sizes (5–7 nm). E_g band gap values around 3.3–3.2 eV were obtained in the solids. UV–vis–DRS spectra showed in the visible region, the silver plasmon surface resonance which intensity was taken as an indirect way to determine the enhanced photoactivity of the semiconductors. In the 4-chlorophenol photodecomposition, it was found that the sol–gel silver fibril solid was more active ($t_{1/2}$ = 57 min) than the silver solid state microbars ($t_{1/2}$ = 92 min). It is proposed that the highest photoactivity showed by the sol–gel fibril preparation is an effect due to the formation of highly dispersed silver nanoparticles on the sol–gel hexatitanate support.

1. Introduction

Pesticides and dyes are the most common pollutants in wastewater, and they are very resistant to conventional biodegradation treatments [1,2]; hence, alternative methods to destroy them are important research subjects around the world. In this way, the photocatalytic degradation using semiconductors as catalysts has been shown as the most promising method for the destruction of pollutants in water [3]. Among the semiconductor catalysts, TiO_2 is by far the most studied photocatalyst showing a high performance for the destruction of polluting compounds [4,5]. Alternatively to TiO_2, the new generation of photocatalytic semiconductors like perovskite, showing a tunnel-like crystal structure [6], emerges with promising results for the photocatalytic decomposition of organic compounds [7,8]. On the other hand, alkali titanates with fibril structures that consist of titanium oxide layers and interlayer cations have also been successfully evaluated in the degradation of chloroform [9], 4-chlorophenol [10] and the synthetic dyes, sulforhodamine and methyl orange, under UV light irradiation [11,12]. In the present paper, the results for the photodegradation of 4-chlorophenol obtained with silver nanoparticles deposited on fibril alkali titanates are reported. Chlorophenol was chosen because it has been reported as an organic molecule that presents a very high resistance to be degraded [1,13]. Silver has been chosen because it has been reported that is a metal that improves the photocatalytic activity of TiO_2 [14], and because it has never been studied as a photoactivity promoter for the alkali titanates. The titanates were obtained by the sol–gel method and solid state reaction. Silver was deposited by using the deposition–precipitation method with NaOH. The semiconductors were characterized by X-ray diffraction (XRD), nitrogen adsorption, UV–vis spectroscopy, scanning electron microscopy (SEM), energy dispersive X-ray spectroscopy (EDS), high resolution transmission electron microscopy (HRTEM) and high angle annular dark field (HAADF).

2. Experimental

2.1. Synthesis of sodium hexatitanate

Sodium hexatitanate ($Na_2Ti_6O_{13}$) was prepared by the sol–gel process and solid state reaction following the methods previously reported [15], in brief; for the sol–gel synthesis, 38.5 g of titanium butoxide (Aldrich, 98%) were added dropwise to a solution

* Corresponding author. Tel.: +52 8183521983x221; fax: +52 8183760477.
E-mail address: vicenrg@hotmail.com (V. Rodríguez-González).

0920-5861/$ – see front matter © 2009 Elsevier B.V. All rights reserved.
doi:10.1016/j.cattod.2009.04.018

containing 8.7 mL of deionized water, 28 mL of ethanol and 3.7 g of sodium tert-butoxide (Aldrich, 97%). The gelling solution was placed under reflux for 72 h at 70 °C with constant stirring. Afterwards, the obtained materials were dried at 100 °C for 12 h, and then annealed in air at 710 °C for 5 h.

The solid state reaction was carried out by mixing Na_2CO_3 (Aldrich, 99%) and TiO_2 (Aldrich, 99.8%), the required stoichiometry for the formation of the sodium hexatitanate ($Na_2Ti_6O_{13}$) was taken into account. Prior to the solid state reaction, the mixed precursors were decarbonated at 710 °C for 5 h. The homogenized solid solution was placed into an electric oven; and then annealed in air at 950 °C for 12 h, using a 1.3 °C/min heating rate.

2.2. Silver nanoparticles stabilized on sodium hexatitanate microfibers

Silver nanoparticles were deposited using the deposition–precipitation method with NaOH (DP-NaOH). The annealed sodium hexatitanate ($Na_2Ti_6O_{13}$) was dispersed in 13 mL of a 7.42×10^{-3} M silver nitrate aqueous solution in order to obtain a final Ag load of 0.5 wt.%. The suspension was heated at 80 °C, then a solution of NaOH (0.5 M) was added until a pH of 9 was reached, thus promoting the precipitation of AgOH on the titanate. The synthesis was performed with vigorous stirring in the dark to avoid the silver decomposition by light effects.

After the silver deposition on the titanates, the solids were separated from the solution by centrifugation. Then, the solids were washed several times with warm distilled water (50 °C) and dried under vacuum for 2 h at 90 °C. Finally, the solids were reduced with hydrogen (500 mL/min) at 200 °C for 2 h in a U glass reactor equipped with a fritted plate with a diameter of 1.5 cm.

All the samples were stored at room temperature in a vacuum desiccator in dark conditions in order to prevent light-induced modifications. The silver semiconductors were identified as STSG and STSS for the silver sodium hexatitanates prepared by the sol–gel route and solid state reaction, respectively.

2.3. Characterization of silver nanoparticles over sodium hexatitanate microfibers

The powder XRD patterns of the stabilized samples were recorded at room temperature on a Bruker D8 Advance diffractometer using Cu Kα radiation (with 2θ ranging from 10° to 70°). The specific surface area of the solids was measured by nitrogen adsorption at −196 °C using a Quantachrome Autosorb 3B automatic instrument. The specific surface area was calculated by the Brunauer–Emmett–Teller method (BET method). Before the nitrogen adsorption, the catalysts were outgassed at 300 °C for 12 h to remove adsorbed impurities. The UV–vis spectra (200–900 nm) of the solids were obtained with a Varian spectrophotometer model Cary 100 (diffuse reflectance mode). Scanning electron microscopy (SEM) observations were performed with a JEOL 6490 LV electron microscope using semiquantitative energy dispersive X-ray spectroscopy (EDS). The thermally treated samples were also examined by TEM in a JEOL JEM-2010 FasTem analytical microscope equipped with a Z contrast annular detector. The powdered samples were dispersed in water and supported on holey carbon coated copper grids. High resolution transmission electron microscopy (HRTEM) and high angle annular dark field (HAADF) digital images were analyzed using Digital Micrograph Software from GATAN™. Histograms of the metal particle sizes were obtained by measuring about 400–500 particles. The size limit for the detection of silver particles was 1 nm. The mean particle size was calculated from the following formula: $=\Sigma nidi/\Sigma ni$, where (ni) is the number of particles with diameter (di).

2.4. Photocatalytic decomposition of 4-chlorophenol

The photocatalytic degradation of 4-chlorophenol (Aldrich, 98%) was performed with a standard Pen-Ray UV lamp (UVP Products) with a typical λ of 254 nm and intensity of 4400 μW/cm^2. The photocatalytic tests were performed in a home-made slurry reactor at room temperature. The lamp was protected with a quartz tube and immersed in a cooled vessel containing the reactant solution (150 mL with 50 ppm of 4-chlorophenol (4-CP) and 150 mg of catalyst). In order to achieve the saturation of dissolved oxygen and to assure the adsorption–desorption equilibrium of the 4-CP on the semiconductor, the suspension was maintained under magnetic stirring in the dark for 60 min with a continuous flow of dry air (1 mL s^{-1}). Then the light source was turned on. The photoactivity degradation rate was followed by measuring the intensity of the absorption band of the 4-CP (224 nm) as a function of the irradiation time with a UV–vis spectrophotometer. Each sample was filtered through a 0.45-μm nylon filter and monitored. For the photocatalytic evaluation, aliquots of the solution were taken every 10 min. The photocatalytic test was performed three times and the experimental error bar was obtained.

3. Results and discussion

The XRD patterns for both hexatitanate powders (sol–gel and solid state) show good crystallinity. In Fig. 1, the sodium hexatitanate crystalline phase, $Na_2Ti_6O_{13}$ (JCPDF 73-1398) can be observed in both samples. It must be mentioned that during the stabilization of the silver sodium hexatitanate samples, the color of the powders changed from white to a grey tone, which is typical of silver composites [16]. The surface specific area determined by N_2

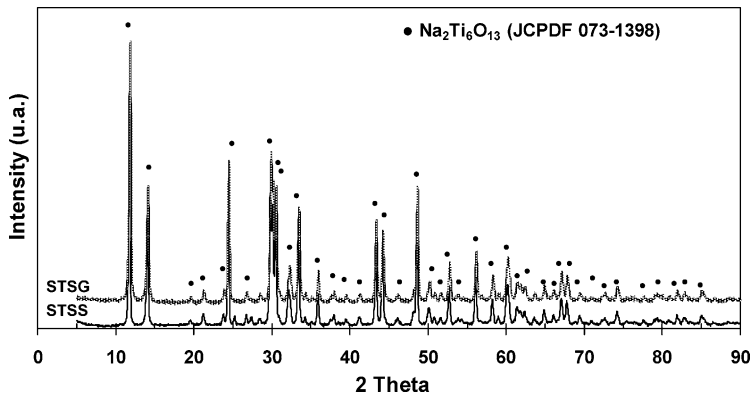

Fig. 1. XRD patterns for silver incorporated into sodium hexatitanates.

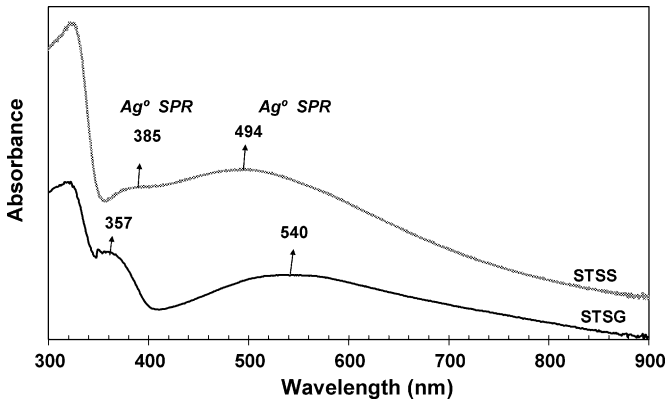

Fig. 2. UV–vis spectra of sodium hexatitanates after the incorporation of silver nanoparticles.

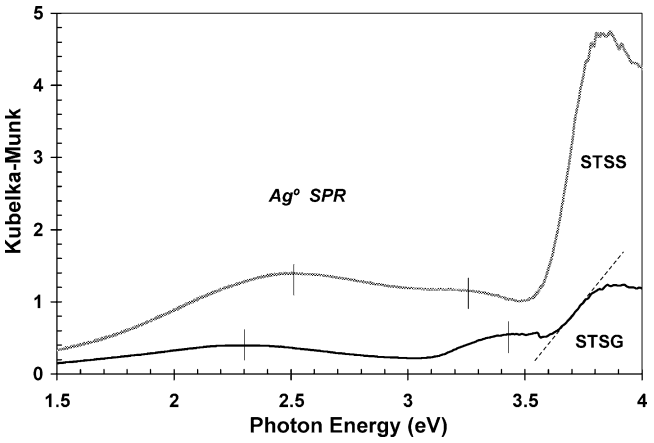

Fig. 3. Kubelka–Munk UV–vis spectra of sodium hexatitanates after the incorporation of silver nanoparticles.

physisorption for both hexatitanate preparations was less than 10 m^2/g and does not varies after the incorporation of the silver nanoparticles.

UV–vis spectra of the silver sodium hexatitanates are presented in Fig. 2. Very similar band gaps of 3.20 and 3.22 eV for the STSG and STSS samples were obtained. These values are in the same order of the band gap for the hexatitanates (Table 1). As for the UV–vis–DRS spectra obtained via the Kubelka–Munk function (Fig. 3), the absorption bands where found shifted to 3.46 and 3.52 eV for the sol–gel hexatitanates, and solid state preparations, respectively (Fig. 2). Silver surface plasmon resonance (SPR) absorption bands can also be seen in the UV–vis spectra at 540 and 494 nm for the sol–gel and solid state preparations, respectively. SPR is observed on silver nanoparticles smaller than 7.0 nm when they are supported on low specific surface area solids, forming closer nanoclusters [17]. A study about the size effect of Ag nanoparticles on surface plasmon resonance [18] reported that the absorption band of silver nanoparticles was less broad and displaced to the

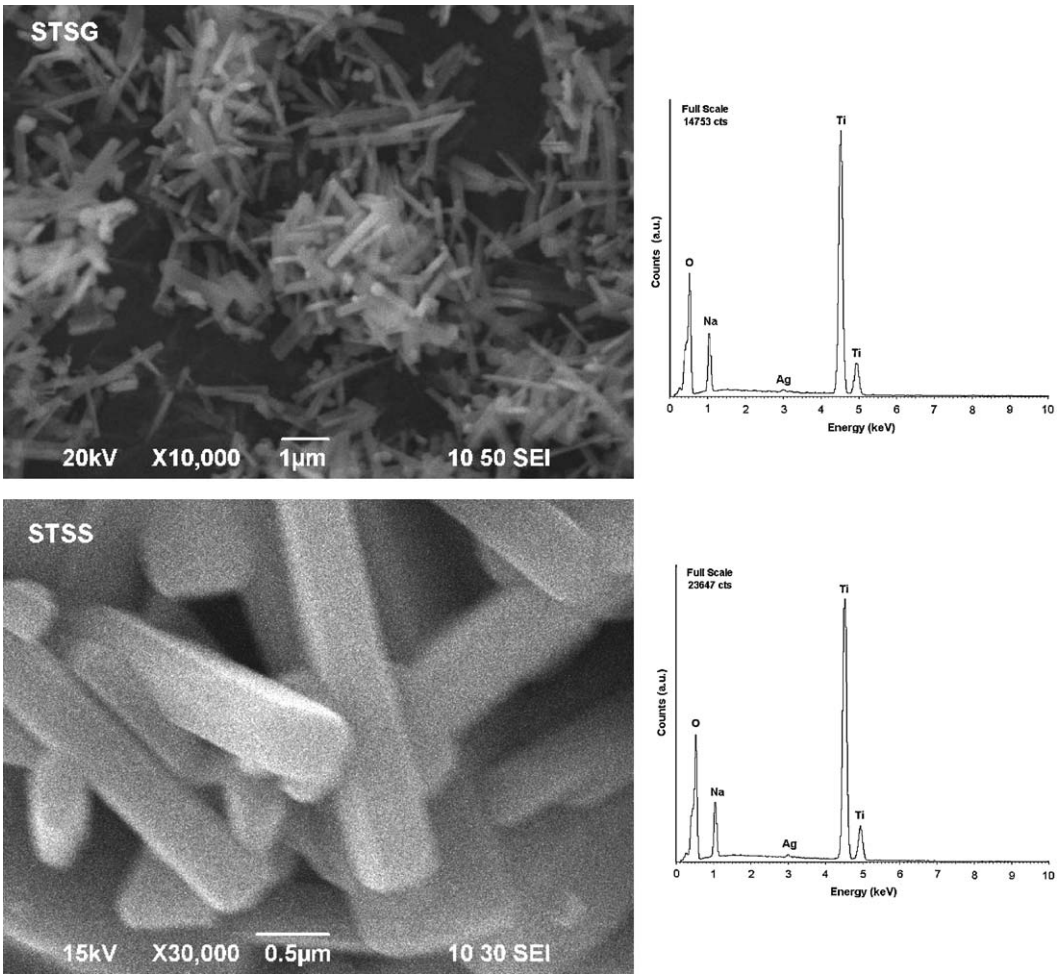

Fig. 4. SEM images for: (a) sol–gel silver loaded sodium hexatitanates and (b) solid state silver loaded sodium hexatitanates.

Table 1
Textural and semiconductor properties of silver-sodium hexatitanates.

Hexatitanate	TSG	TSS	STSG	STSS
E_g (eV)	3.26	3.30	3.20	3.22
E_g (eV) K–M[a]	–	–	3.46	3.52
Main band SPR[b] Absorbance/K–M (nm/eV)	–	–	540/2.5	494/2.3
Ag particle size (nm)	–	–	5.5	6.5

[a] Kubelka–Munk function.
[b] Surface plasmon resonance absorption.

visible region as the size of the silver nanoparticles decreased. However, in a recent study on gold nanoparticles deposited by a similar method on different supports, the SPR absorption was found to be more important when the gold particle size was increased [19].

With the aim to disclose particle size effects on the SPR induced by the DP-NaOH preparation method, SEM–EDS and HAADF–STEM observations were performed. The SEM images (Fig. 4) show the microstructural morphology of silver loaded sodium hexatitanates. The silver loaded sol–gel hexatitanates show homogenously distributed microfibers with a mean size of about 0.2 μm × 3 μm. For the solid state preparation, hexatitanates showing octagonal microbars of 0.4 μm × 5 μm are observed. By using semiquantitative energy dispersive X-ray spectroscopy (EDS) in both materials, the peak denoting the presence of silver was identified but with a very low intensity (0.5 Ag wt.%). HRTEM of the STSG sample shows egg-shaped silver nanoparticles (5.2 nm × 7.8 nm) deposited over the hexatitanate (Fig. 5). From Fig. 5a, the lattice fringes coincide with the interplanar spacing for $Na_2Ti_6O_{13}$ ($d_{1\,1\,1}$ = 3.325 Å JCPDF 73-1398). A selected cylindrical microfiber is shown in Fig. 5b, where some silver nanoparticles over the microfiber (d = 125 nm) can be distinguished. In the HAADF–STEM mode, silver nanoparticles with a mean size of 5.5 nm can be seen (Fig. 5c). For the STSS silver loaded-microbar sample, the size of the microbars was about 5 μm in length and 0.5 μm in diameter (Fig. 6a–c). The mean particle size of the silver nanoparticles was around 6.5 nm.

In the photodecomposition of 4-CP all the catalysts followed pseudo-first-order kinetics and the apparent rate constant was calculated by plotting $\ln(C_0/C)$ versus time. The slope of the plot represents the apparent rate constant K (Table 2). The corresponding activities are reported as $t_{1/2}$ in Table 2. The photocatalytic decomposition of 4-CP using TSG and TSS hexatitanates reaches after 160 min in irradiation photodecomposition percentages of 87 and 78%, respectively. For the STSG sample the photodecomposition increases to 95%, meanwhile, with the STSS sample, a photodegradation similar to that of the hexatitanate support (72%) was observed (Figs. 7 and 8). This behavior can be explained by the fact that the intensity of the silver SPR absorption for the STSG samples was lower than that obtained with the STSS samples (Figs. 2 and 3). As it was previously mentioned for silver metallic nanoparticles showing analogous particle sizes, the differences in

Table 2
Photoactivity and kinetic parameters for the 4-chlorophenol degradation over silver sodium hexatitanates.

Titanate	%C[a]	$t_{1/2}$[b] (min)	K[c] ($min^{-1}\,g^{-1}$)
Photolysis	69	100	–
TSS	78	96	0.0072
STSS	72	92	0.0075
TSG	87	76	0.0091
STSG	95	57	0.0122

[a] % of conversion of 4-CP at 160 min.
[b] Half time at 160 min.
[c] Kinetic rate constant.

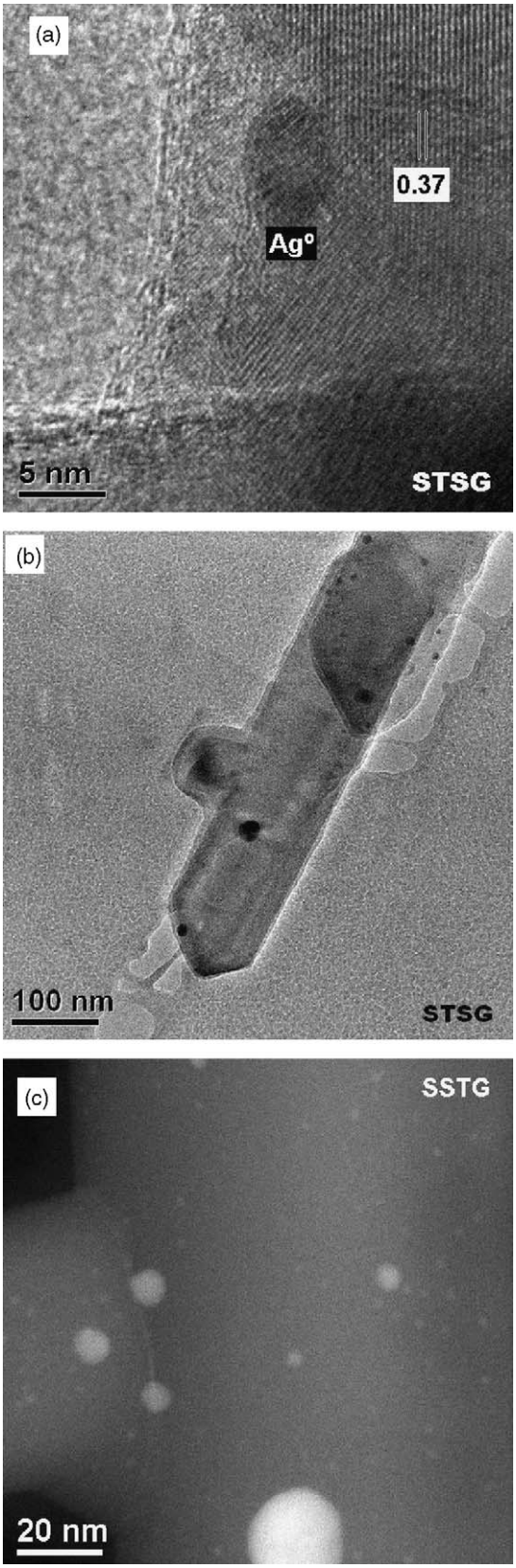

Fig. 5. Silver loaded sodium hexatitanate HRTEM image (a), and STEM Z contrast images for the STSG semiconductor (b and c).

the intensity of the SPR absorption could only be explained by the effect of the interaction between neighboring particles. On the STSG sample, the silver metallic particles are highly dispersed and neighboring effects do not significantly contribute to the intensity

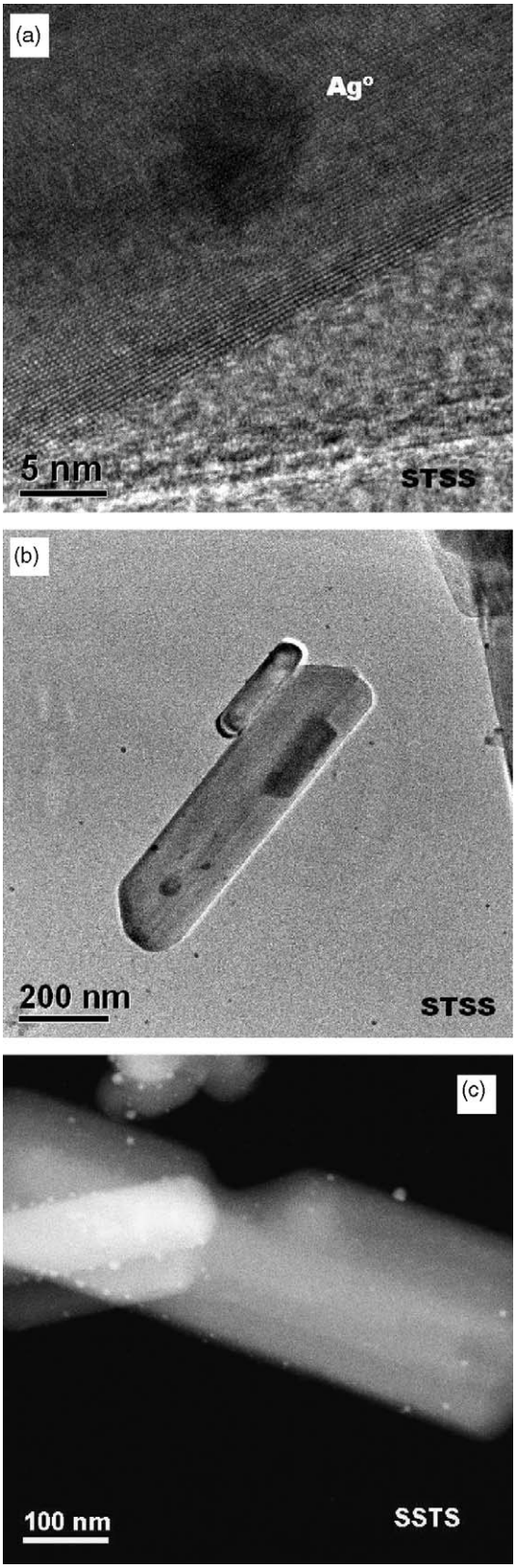

Fig. 6. Silver loaded sodium hexatitanate semiconductor HRTEM images (a), STEM Z contrast images for the STSS semiconductor (b and c).

of the SPR absorption. In the case of the STSS photocatalysts, the silver particles are closer on the support showing an increase in the SPR absorption intensity. The high intensity of the band on the silver SPR absorption is produced by the delocalization of electrons

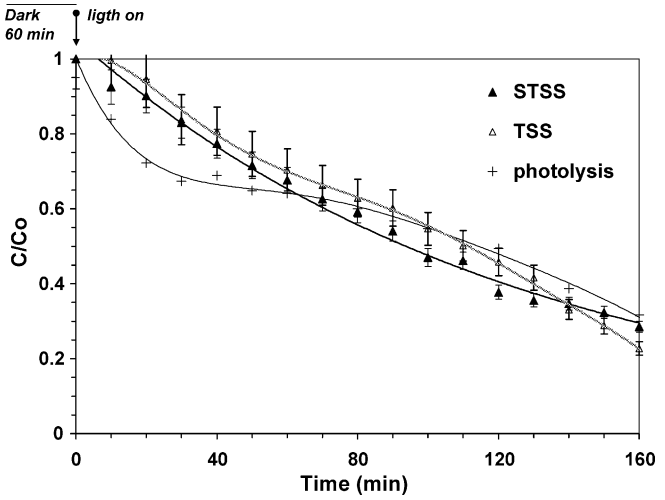

Fig. 7. Photocatalytic degradation of 4-chlorophenol as a function of time for the STSS semiconductor.

in the metal bulk and a possible reflectivity of the irradiated light during the photocatalytic process could be present. Thus, the different silver SPR absorptions showed by both samples certainly is an effect of the method used for the preparation of the hexatitanate supports. By the solid state method, large microbars were formed and then closer silver clusters were obtained, whereas by means of the sol–gel method, narrow fibers were formed and hence the silver nanoparticles are largely dispersed. These results are of great importance because this is the first time that it is assumed that the closeness of the neighboring silver nanoparticles plays a major role in the photodegradation of chlorophenol. Among the various metallic properties, the delocalization of electrons in bulk metals allows light reflectivity and SPR absorption. Both the reflectivity and silver SPR absorption effects are not present in high dispersed metallic nanoparticles smaller than 6 nm. Then, the surface plasmon resonance absorption intensity will be an indirect way to determine the photoactivity improvement promoted by the nanoparticles.

The 4-chlorophenol photodecomposition using sodium hexatitanates has been recently reported [10]. In such article the authors used a UV lamp with a 365 nm light source. In the present work, a UV lamp with a 254 nm light source was used. In Ref. [10] the photodegradation of a solution containing

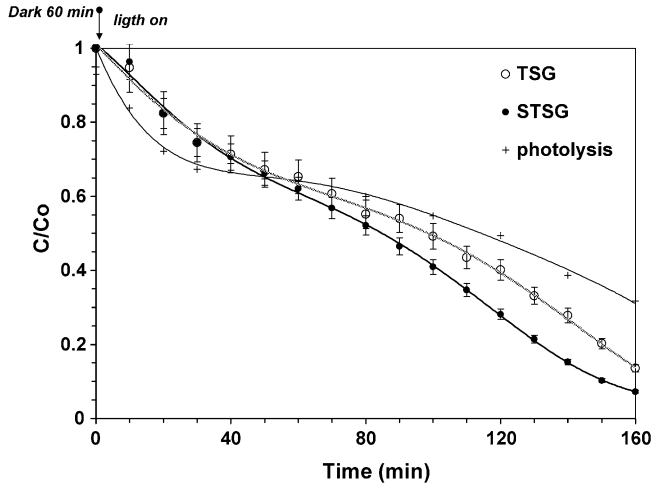

Fig. 8. Photocatalytic degradation of 4-chlorophenol as a function of time for the STSG semiconductor.

1.0×10^{-4} M of 4-chlorophenol was carried out. In our case, a solution with 3.8×10^{-4} M was used. With these very different experimental work conditions, the comparison between both photocatalytic systems cannot be established. However, with our photocatalysts we reached 95% of 4-cholophenol converted in a time lower than 3 h, meanwhile in the referred article the authors required more than 3 h to degrade a solution with a lower concentration of the organic pollutant. Thus the presence of silver deposited on the hexatitanates notably improved the photocatalytic efficiency.

4. Conclusions

Sodium hexatitanates (fibrils or microbars) were obtained depending on the method used in their preparation, sol–gel or solid state reaction respectively. XRD data as well as electron microscopy observations confirm the formation of the $Na_2Ti_6O_{13}$ crystalline solid. For silver loaded hexatitanates, surface plasmon resonance absorption with different intensities was obtained. For the SG sodium hexatitanate, the SPR absorption was broad and with low intensity, meanwhile the SS preparation showed a SPR with high intensity. It is showed that the sol–gel silver sodium hexatitanate fibrils are more active ($t_{1/2}$ = 57 min) in the 4-chlorophenol photodegradation than the silver sodium hexatitanate microbars synthesized by the solid state reaction ($t_{1/2}$ = 98 min). It is assumed that the photoactivity enhancement found in the SG silver solid was due to the highly dispersed silver nanoparticles formed on the hexatitanate fibril semiconductor.

Acknowledgements

The authors would like to thank to "Fundación UANL" and the administration of Civil Engineering Faculty (UANL) for the financial support. Also we appreciated the synthesis help, and the technical assistance given by Erika I. Cedillo González and Luis Rendón (LCM-IF, HRTEM). V. Rodríguez González would like to thank the PROMEP program 103.5/08/3125 UANL-PTC-244 project. R. Zanella acknowledges PUNTA (IMPULSA 01) and CONACYT 55154 projects for the financial support.

References

[1] S. Chiron, A. Fernández-Alba, A. Rodríguez, E. García-Calvo, Water Res. 34 (2000) 366.
[2] C. Hachem, F. Bocquillon, O. Zahraa, M. Bouchy, Dyes and Pigments 49 (2001) 117.
[3] A. Fujishima, T.N. Rao, D.A. Tryk, J. Photochem. Photobiol. C: Photochem. Rev. 1 (2000) 1.
[4] E. Vulliet, J.-M. Chovelon, C. Guillard, J.-M. Herrmann, J. Photochem. Photobiol. A: Chem. 159 (2003) 71.
[5] O.G. Granados, O.C.A. Paéz, M.F. Martínez, O. Edgar, A. Paéz-Mozo, Catal. Today 107–108 (2005) 589.
[6] H.W. Eng, P.W. Barnes, B.M. Auer, P.M. Woodward, J. Solid State Chem. 175 (2003) 94.
[7] Y. Yang, Y. Sun, Y. Jiang, Mater. Chem. Phys. 96 (2006) 234.
[8] H. Song, H. Jiang, T. Liu, X. Liu, G. Meng, Mater. Res. Bull. 42 (2007) 334.
[9] N. Bao, L. Shen, K. Yanagisawa, J. Phys. Chem. B 108 (2004) 16739.
[10] V. Stengl, S. Bakardjieva, J. Subrt, E. Vecernikova, L. Szatmary, M. Klementova, V. Balek, Appl. Catal. B 63 (2006) 20–30.
[11] H. Zhu, X. Lan, D. Song, Y. Xi, J. Zhao, J. Am. Chem. Soc. 126 (2004) 8380.
[12] N. Venkatachalam, M. Palanichamy, V. Murugesan, J. Mol. Catal. A: Chem. 273 (2007) 177.
[13] M.K. Seery, R. George, P. Floris, S.C. Pillai, J. Photochem. Photobiol. A: Chem. 189 (2007) 258.
[14] S.G. Hur, T.W. Kim, S.-J. Hwang, J.-H. Choy, J. Photochem. Photobiol. A: Chem. 183 (2006) 176.
[15] V. Rodríguez-González, I. Juárez-Ramírez, R. Zanella, M.E. Zarazúa, L.M. Torres-Martínez, J. Ceram. Process. Res. 9 (2008) 601–605.
[16] B. Ohtani, S.W. Zhang, T. Ogita, S. Nishimoto, T. Kagiya, J. Photochem. Photobiol. A: Chem. 71 (1993) 195.
[17] P.V. Kamat, J. Phys. Chem. B 106 (2002) 7729.
[18] K.-C. Lee, S.-J. Lin, C.-H. Lin, C.-S. Tsai, Y.-J. Lu, Surf. Coat. Technol. 202 (2008) 5339.
[19] V. Rodríguez-González, R. Zanella, G. del Ángel, R. Gómez, J. Mol. Catal. A: Chem. 281 (2008) 93.